第9章　古典力学の散乱理論

散乱理論は量子力学でもその取扱いはかなり難しいものである．古典力学においては散乱理論の厳密な定式化が可能かどうか良く分からない．しかし古典力学における散乱断面積は直感的にはわかり易いとも言えるので，ここで少し散乱理論に慣れておくことは無駄にはならないと思われる．ここではまず剛体との弾性散乱における散乱断面積について解説しよう．そしてその後，Rutherford 散乱の微分断面積を計算しよう．これは勿論，量子論的な散乱理論を勉強するために多少の手助けにはなると期待して解説しているものである．

9.1　剛体との弾性散乱

質点が半径 R の剛体と散乱する場合の散乱断面積を求めてみよう．そして散乱断面積の計算結果が

$$\sigma = \pi R^2 \tag{9.1}$$

となる事を示して行こう．まず，衝突パラメータ (impact parameter) と言う物理量を導入しよう．これは図のように b を衝突パラメータと定義している．この場合，微分断面積は

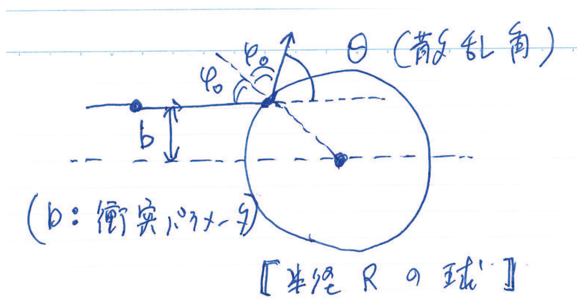

図 9.1: 剛体との散乱

$$d\sigma = d^2b = bdbd\varphi = 2\pi bdb \tag{9.2}$$

となる．この衝突パラメータ b は入射粒子の速度の方向を z 軸とした場合，円筒座標の２次元平面座標 r に対応している．

今の場合，散乱過程で φ の依存性はない．従って φ の積分ができて 2π が出ている．微分断面積 $d\sigma$ を求めるためには，まず衝突パラメータ b と粒子の散乱角 θ とを関係づける必要がある．よって式 (9.2) を

$$d\sigma = d^2b = bdbd\varphi = 2\pi b \left|\frac{db}{d\theta}\right| d\theta \tag{9.3}$$

と書き直そう．絶対値を付けたのは断面積が正の値を取るからである．図 9-1 から

$$2\varphi_0 + \theta = \pi \tag{9.4}$$

である．よって

$$b = R\sin\varphi_0 = R\cos\frac{\theta}{2} \tag{9.5}$$

となる．これより

$$\frac{db}{d\theta} = -\frac{R}{2}\sin\frac{\theta}{2} \tag{9.6}$$

である．よって微分断面積は

$$d\sigma = 2\pi b \left|\frac{db}{d\theta}\right| d\theta = \frac{\pi}{2}R^2\sin\theta d\theta \tag{9.7}$$

となる．ここで立体角 $d\Omega$ を

$$d\Omega = \sin\theta d\theta d\varphi$$

とすれば微分断面積は

$$\frac{d\sigma}{d\Omega} = \frac{1}{4}R^2 \tag{9.8}$$

となっている．これより剛体散乱の全断面積は

$$\sigma = \pi R^2 \tag{9.9}$$

となる．これは半径 R の球を遠方から見た時の断面積である．

9.2 Rutherford 散乱

荷電粒子が原子核と散乱する過程は Rutherford 散乱と呼ばれている．これは原子核が作るクーロン場 $U(r) = \frac{\alpha}{r}$ と荷電粒子とのクーロン散乱であり，散乱理論の定番でもある．この微分断面積は量子力学における散乱理論によって記述されているが古典力学の手法でも微分断面積が正しく求まっている．ここではその計算を紹介しよう．

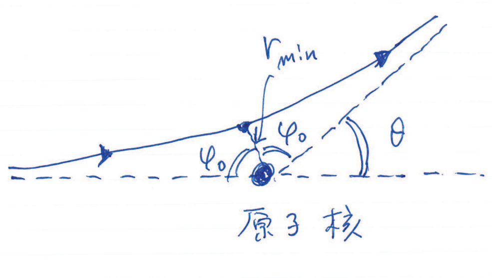

図 9.2: Rutherford 散乱

原子核が作るクーロンポテンシャルは $\alpha = Ze$ なので

$$U(r) = \frac{Ze}{r} \tag{9.10}$$

である．ここではこの Rutherford 散乱の微分断面積を求めて行こう．最初にその結果を書いておこう．この微分断面積は

$$\frac{d\sigma}{d\Omega} = \left(\frac{\alpha}{2mv^2}\right)^2 \frac{1}{\sin^4\frac{\theta}{2}} \tag{9.11}$$

と書かれている．ここで v は入射粒子の速度である．

9.2.1 角運動量の保存

この散乱においては中心力との散乱であるため，角運動量 L は保存する．この場合，角運動量 L は

$$\boldsymbol{L} = \boldsymbol{r} \times m\boldsymbol{v} \tag{9.12}$$

である．図 9-1 からこの質点の角運動量の大きさ L は

$$L = mbv \tag{9.13}$$

となっている．

9.2.2 φ_0 の計算

クーロンポテンシャルの場合，その軌道を与える方程式は

$$\frac{dr}{d\varphi} = \frac{r^2}{L}\sqrt{2m\left(E - \frac{\alpha}{r} - \frac{L^2}{2mr^2}\right)} \tag{9.14}$$

であった．ここで図 9-2 から φ_0 は

$$\varphi_0 = \int_{r_{min}}^{\infty} \frac{\frac{L}{r^2}dr}{\sqrt{2m\left(E - \frac{\alpha}{r} - \frac{L^2}{2mr^2}\right)}} \tag{9.15}$$

となる．ここで r_{min} は荷電粒子が原子核に最も近付いた時の距離である．この積分の計算はすでに Kepler 問題のところで解説しているので，ここではその結果だけを書いておこう．この場合，この積分は

$$\cos\varphi_0 = \frac{\frac{\alpha}{E}}{\sqrt{\left(\frac{\alpha}{E}\right)^2 + \frac{2L^2}{mE}}} \tag{9.16}$$

となっている．ここで

$$E = \frac{1}{2}mv^2, \qquad L = mbv \tag{9.17}$$

を使うと

$$\cos\varphi_0 = \frac{1}{\sqrt{1 + \left(\frac{mv^2b}{\alpha}\right)^2}} \tag{9.18}$$

と求まる．これより

$$\tan\varphi_0 = \frac{mv^2b}{\alpha} \tag{9.19}$$

となり，φ_0 を衝突パラメータ b と関係づける事が出来ている．

一方，図 9-2 より

$$\varphi_0 = \frac{\pi}{2} - \frac{\theta}{2} \tag{9.20}$$

なので，これより

$$b = \frac{\alpha}{mv^2} \cot \frac{\theta}{2} \tag{9.21}$$

である．式 (9.2) で定義されているように，散乱の微分断面積は

$$d\sigma = b \left| \frac{db}{d\theta} \right| \frac{d\Omega}{\sin\theta} \tag{9.22}$$

となっている．ここで式 (9.21) を使って上式の計算を実行すれば Rutherford 散乱の微分断面積が求まる．それは

$$\frac{d\sigma}{d\Omega} = \left(\frac{\alpha}{2mv^2} \right)^2 \frac{1}{\sin^4 \frac{\theta}{2}} \tag{9.23}$$

と書かれている．この結果は量子論の散乱理論で計算された Rutherford 散乱の微分断面積と一致している．しかしながら，この一致はクーロンポテンシャルの特殊性に依っているものと考えられる．実際，剛体との散乱の場合，古典論の結果は量子力学の計算とは少し異なったものである事が知られている．

第13章　量子論における散乱理論

量子力学における散乱理論を解説する事は決して易しい事ではない．その説明にはそれだけで１冊の本が必要であると考えられる．さらに散乱理論はかなり難しいとも言える理論体系である．量子論において束縛状態を解く事はそれ程難しいとは言えないのだが，散乱状態を扱う事は波の広がりがマクロスケールになるため，非常に難しくなっているのである．しかし実験と理論を結び付ける場合，基本的には散乱理論を使う事になっている．粒子をターゲットにぶつけてその散乱における反応を見て行く事が実験物理学の基本である事に依っている．この事から考えても，散乱理論の重要性が理解できるであろう．

古典力学における散乱理論を第９章で簡単に紹介しているが，ここでは量子力学における散乱理論 (但しポテンシャル散乱に限定) を解説しよう．この章では主に Eikonal 近似と言われている手法による散乱断面積の計算法を紹介しよう．この方法は Glauber 理論ともよばれている理論模型であるが，ある条件下での散乱断面積の記述には非常に有効である事が分かっている．利用価値が高い割には取り扱いが簡単であるため，幅広く応用されている散乱理論である．

13.1　散乱振幅 $f(\boldsymbol{q})$

散乱振幅 $f(\boldsymbol{q})$ について簡単に説明しよう．この散乱振幅は質量 m の粒子が入射エネルギー E_k を持っている場合，その粒子が他の粒子が作るポテンシャル $V(\boldsymbol{r})$ によるポテンシャル散乱の散乱断面積を記述する時の基本的な物理量である．この場合，Hamiltonian H は

$$H = -\frac{1}{2m}\boldsymbol{\nabla}^2 + V(\boldsymbol{r}) \tag{13.1}$$

である．

従って Schrödinger 方程式は

$$\left(-\frac{1}{2m}\boldsymbol{\nabla}^2 + V(\boldsymbol{r})\right)\psi(\boldsymbol{r}) = E_k\psi(\boldsymbol{r}) \tag{13.2}$$

となっている．但し，これは固有値方程式ではない．実際，E_k は入射エネルギーであり，与えられている物理量である．この Schrödinger 方程式から Lippmann-Schwinger 方程式を求める事が出来る．これは

$$\psi = \phi + \frac{1}{E_k - H_0 + i\varepsilon}V\psi \tag{13.3}$$

と書かれている．ここで ϕ は自由粒子の解であり，H_0 は自由粒子の Hamiltonian である．よって

$$\phi(\boldsymbol{r}) = e^{ikz}, \qquad k = \sqrt{2mE_k} \tag{13.4}$$

$$H_0 = -\frac{1}{2m}\boldsymbol{\nabla}^2 \tag{13.5}$$

となっている．この場合，入射粒子は z 方向に入射していると仮定されている．また $+i\varepsilon$ は外向きの波を表すために導入されたものである．

13.1.1 伝搬関数

Lippmann-Schwinger 方程式において

$$\frac{1}{E_k - H_0 + i\varepsilon} \tag{13.6}$$

は演算子となっているが，これは伝搬関数に対応している．ここで

$$G(\boldsymbol{r}, \boldsymbol{r}') = \langle\boldsymbol{r}|\frac{1}{E_k - H_0 + i\varepsilon}|\boldsymbol{r}'\rangle \tag{13.7}$$

としよう．この伝搬関数は運動量 $\boldsymbol{p}$ の完全系を中間状態に挿入すると

$$G(\boldsymbol{r}, \boldsymbol{r}') = \int \frac{d^3p}{(2\pi)^3}\,\frac{1}{E_k - \frac{p^2}{2m} + i\varepsilon}e^{\boldsymbol{p}\cdot(\boldsymbol{r}-\boldsymbol{r}')} \tag{13.8}$$

となる．この運動量積分ではまず角度積分がすぐに実行できて

$$G(\boldsymbol{r}, \boldsymbol{r}') = -\frac{m\pi}{2\pi^2|\boldsymbol{r}-\boldsymbol{r}'|}\,\mathrm{Im}\int_{-\infty}^{\infty} dp\,\frac{e^{ip\,|\boldsymbol{r}-\boldsymbol{r}'|}}{p^2 - k^2 - i\varepsilon} \tag{13.9}$$

となる．この p 積分は複素平面における積分計算を実行すればよく，その結果

$$G(\boldsymbol{r}, \boldsymbol{r}') = -\frac{m}{2\pi|\boldsymbol{r}-\boldsymbol{r}'|} e^{ik\,|\boldsymbol{r}-\boldsymbol{r}'|} \tag{13.10}$$

と求まる．さらに今の場合，$r \gg r'$ なので

$$|\boldsymbol{r}-\boldsymbol{r}'| = r - \frac{(\boldsymbol{r}\cdot\boldsymbol{r}')}{r} + \cdots \tag{13.11}$$

は充分良い近似である．よって

$$G(\boldsymbol{r}, \boldsymbol{r}') = -\frac{m}{2\pi r}\, e^{ikr}\, e^{-i\boldsymbol{k}'\cdot\boldsymbol{r}'} \tag{13.12}$$

と求まっている．但し k' は

$$\boldsymbol{k}' = k\hat{\boldsymbol{r}} \tag{13.13}$$

と定義されている．これより式 (13.3) は

$$\begin{aligned}\psi(\boldsymbol{r}) &= e^{ikz} - \frac{m}{2\pi}\frac{e^{ikr}}{r}\int e^{-i\boldsymbol{k}'\cdot\boldsymbol{r}'} V(\boldsymbol{r}')\psi(\boldsymbol{r}') d^3r' \\ &= e^{ikz} + f(\boldsymbol{q})\frac{e^{ikr}}{r}\end{aligned} \tag{13.14}$$

となる．この場合，散乱振幅 $f(\boldsymbol{q})$ は

$$f(\boldsymbol{q}) = -\frac{m}{2\pi}\int e^{-i\boldsymbol{k}'\cdot\boldsymbol{r}'} V(\boldsymbol{r}')\psi(\boldsymbol{r}') d^3r' \tag{13.15}$$

と定義されている．但し $\boldsymbol{q} = \boldsymbol{k} - \boldsymbol{k}'$ である．

13.1.2 Lippmann-Schwinger 方程式の導出

ここで Lippmann-Schwinger 方程式を導出しよう．まずは Schrödinger 方程式

$$(E_k - H_0)\psi = V\psi \tag{13.16}$$

に対して左から演算子

$$(E_k - H_0 + i\varepsilon)^{-1} \tag{13.17}$$

を掛ける．$+i\varepsilon$ を入れたのは分母がゼロとなる事を防ぐためである．この時，式 (13.16) は

$$\psi = \frac{1}{E_k - H_0 + i\varepsilon} V\psi \tag{13.18}$$

となる．一方，自由粒子の方程式は

$$(E_k - H_0)\phi = 0 \tag{13.19}$$

である．従って，式 (13.18) に自由粒子の解 ϕ を足して置く必要がある．よって

$$\psi = \phi + \frac{1}{E_k - H_0 + i\varepsilon} V\psi \tag{13.20}$$

となり，これが Lippmann-Schwinger 方程式である．前述したように，分母の $+i\varepsilon$ は散乱波が外向きの波 $[e^{ikr}]$ であると言う境界条件を課した事に対応している．

13.1.3 T 行列

式 (13.20) に左から V を掛けて ϕ で期待値を取ると

$$\langle\phi|V|\psi\rangle = \langle\phi|V|\phi\rangle + \langle\phi|V\frac{1}{E_k - H_0 + i\varepsilon}V|\psi\rangle \tag{13.21}$$

となる．ここで T 行列を

$$T = \langle\phi|V|\psi\rangle \tag{13.22}$$

と定義すると式 (13.21) は

$$T = V + V\frac{1}{E_k - H_0 + i\varepsilon}T \tag{13.23}$$

となる．これが T 行列に対する散乱の方程式である．

13.2　微分断面積 $\left(\frac{d\sigma}{d\Omega}\right)$

微分断面積 $d\sigma$ を定義しよう．これは flux 間の比

$$d\sigma \equiv \frac{\text{散乱波の flux } j_r \text{ at } r^2 d\Omega}{\text{入射波の flux } j_{in}} \tag{13.24}$$

として定義されている．まずは散乱波の flux j_r を計算しよう．この場合，散乱波の波動関数は式 (13.14) の右辺第２項を ψ_r として

$$\psi_r = f(\boldsymbol{q})\frac{e^{ikr}}{r} \tag{13.25}$$

となっている．よって

$$j_r = \frac{1}{2mi}\left(\psi_r^*\frac{\partial\psi_r}{\partial r} - \frac{\partial\psi_r^*}{\partial r}\psi_r\right) = \frac{k}{mr^2}|f(\boldsymbol{q})|^2 \tag{13.26}$$

である．一方，入射波の flux j_{in} は

$$j_{in} = \frac{k}{m} \tag{13.27}$$

である．よって微分断面積は

$$\frac{d\sigma}{d\Omega} = |f(\boldsymbol{q})|^2 \tag{13.28}$$

となっている．ここで $\boldsymbol{q}^2 = 2k^2(1-\cos\theta)$ である．

13.2.1　散乱振幅の求め方：Born 近似

散乱振幅が分かれば散乱断面積が計算できる．しかしこの散乱振幅 $f(\boldsymbol{q})$ は

$$f(\boldsymbol{q}) = -\frac{m}{2\pi}\int e^{-i\boldsymbol{k}'\cdot\boldsymbol{r}'}V(\boldsymbol{r}')\psi(\boldsymbol{r}')d^3r' \tag{13.29}$$

なので Schrödinger 方程式を解いて $\psi(\boldsymbol{r})$ を求める必要がある．これが散乱断面積を計算する時の難しさである．従ってまずは簡単に断面積を求めるために，$\psi(\boldsymbol{r})$ を $\psi(\boldsymbol{r}) = e^{i\boldsymbol{k}\cdot\boldsymbol{r}}$ と自由粒子の解で近似する手法が採用されている．この場合

$$f_B(\boldsymbol{q}) = -\frac{m}{2\pi}\int e^{i\boldsymbol{q}\cdot\boldsymbol{r}'}V(\boldsymbol{r}')d^3r' \tag{13.30}$$

と書かれる．これは Born 近似と呼ばれている方法であり良く使われている．特に，クーロンポテンシャル $V(r) = \frac{\alpha}{r}$ の場合は正しい断面積が得られている．

13.3　部分波展開

散乱理論を扱う場合，散乱振幅を部分波に展開してその性質を議論する事が良くある．これはその方が議論しやすい場合が実際にあるからである．ここでは基本的な数式が天下り的になっているが，詳しい解説は散乱理論の教科書を参考にして貰う事にしよう．ここでは散乱振幅の部分波展開に関する解説を行う事により，散乱理論では非常に重要な役割を果たしている Optical Theorem を証明しよう．

散乱振幅 $f(\boldsymbol{q})$ は

$$f(\boldsymbol{q}) = \frac{i}{2k}\sum_{\ell=0}^{\infty}(2\ell+1)(1-e^{2i\delta_\ell})P_\ell(\cos\theta) \tag{13.31}$$

と部分波展開する事ができる．ここで δ_ℓ は phase shift と呼ばれる量である．また $P_\ell(\cos\theta)$ は Legendre 関数である．この場合，散乱全断面積 σ_T は

$$\sigma_T = \int |f(\boldsymbol{q})|^2 d\Omega \tag{13.32}$$

である．これに式 (13.31) を代入して計算すると

$$\sigma_T = \frac{4\pi}{k^2}\sum_{\ell=0}^{\infty}(2\ell+1)\sin^2\delta_\ell \tag{13.33}$$

と求まる．一方，散乱振幅の式 (13.31) から

$$\mathrm{Im}f(0) = \frac{1}{k}\sum_{\ell=0}^{\infty}(2\ell+1)\sin^2\delta_\ell \tag{13.34}$$

と求まっている．これら２式を比較する事により

$$\sigma_T = \frac{4\pi}{k}\,\mathrm{Im}f(0) \tag{13.35}$$

が示された．これは Optical Theorem (光学定理) として知られている方程式である．この定理は散乱 S 行列の Unitarity と関係しており，非常に重要な式である．

13.4 Eikonal 近似法

半世紀以上前から，Eikonal 近似法を用いた Glauber 理論が良く知られている．これは前方散乱の場合に応用できる理論模型である．またこの模型は多重散乱にも応用されていて，予想以上に実験結果をうまく再現できる模型となっている．この模型はかなり過激な近似をしているにもかかわらず，自然現象の記述には力を発揮すると言う模型である．この理由としては，恐らくは Optical Theorem (光学定理) を満たしていると言う事が一つの要因であろうと考えられる．しかし何故，近似以上にうまく現象を記述できるのかと言う問題の詳しい検証は今後の課題としておこう．

Eikonal 近似の基本は散乱が基本的には直線で起こっていると言う仮定である．この場合，縦方向の運動量 (longitudinal momentum) は散乱前後で不変であるとしている．従って，エネルギー保存がそれに応じて破れている．まずはその近似法を解説しよう．出発点の方程式は勿論，Schrödinger 方程式である．これは

$$\left(-\frac{1}{2m}\boldsymbol{\nabla}^2 + V(\boldsymbol{r})\right)\psi(\boldsymbol{r}) = E_k\psi(\boldsymbol{r}) \tag{13.36}$$

であるが，ここで直線近似を表現するために

$$\psi(\boldsymbol{r}) = e^{ikz}\phi(\boldsymbol{r}) \tag{13.37}$$

としよう．この時，$\phi(\boldsymbol{r})$ に対する方程式は

$$-\frac{ik}{m}\frac{\partial\phi(\boldsymbol{r})}{\partial z} + V(\boldsymbol{r})\phi(\boldsymbol{r}) = \frac{1}{2m}\boldsymbol{\nabla}^2\phi(\boldsymbol{r}) \tag{13.38}$$

となる．ところが上式の右辺は k と比べて充分小さい事が示されるので無視する事が出来る．よって，Eikonal 近似をした方程式は

$$\frac{ik}{m}\frac{\partial\phi(\boldsymbol{r})}{\partial z} = V(\boldsymbol{r})\phi(\boldsymbol{r}) \tag{13.39}$$

となっている．この微分方程式は直ちに解く事が出来て

$$\phi(\boldsymbol{r}) = Ae^{-\frac{m}{k}i\int^z V(\boldsymbol{b},w)dw} \tag{13.40}$$

となる．但し

$$\boldsymbol{r} = (\boldsymbol{b}, z) \tag{13.41}$$

として b を導入している．この b は impact parameter に対応している．

これより ψ は

$$\psi(\boldsymbol{r}) = e^{ikz - \frac{im}{k}\int^z V(\boldsymbol{b},w)dw} \tag{13.42}$$

となる．この場合，規格化定数 A は入射波に合わせて $A=1$ としている．従って散乱振幅 $f(q)$ は式 (13.15) より

$$f(\boldsymbol{q}) = -\frac{m}{2\pi}\int d^3r\, e^{-i\boldsymbol{k}'\cdot\boldsymbol{r}}V(\boldsymbol{r})e^{ikz-\frac{im}{k}\int^z V(\boldsymbol{b},w)dw} \tag{13.43}$$

$$= -\frac{m}{2\pi}\int d^2b\, e^{i\boldsymbol{q}\cdot\boldsymbol{b}} \times \int_{-\infty}^{\infty} dz V(\boldsymbol{b},z)e^{-\frac{im}{k}\int^z V(\boldsymbol{b},w)dw} \tag{13.44}$$

となっている．この場合，$\boldsymbol{k}'\cdot\boldsymbol{r} - kz = -\boldsymbol{q}\cdot\boldsymbol{b}$ を使っている．ここで

$$G(\boldsymbol{b}) = \int_{-\infty}^{\infty} dz V(\boldsymbol{b},z)e^{-\frac{im}{k}\int^z V(\boldsymbol{b},w)dw} \tag{13.45}$$

と置く．これは

$$G(\boldsymbol{b}) = -\frac{k}{im}\int_{-\infty}^{\infty} dz\left(\frac{\partial}{\partial z}e^{-\frac{im}{k}\int^z V(\boldsymbol{b},w)dw}\right) \tag{13.46}$$

$$= \frac{ik}{m}\left[e^{-\frac{im}{k}\int_{-\infty}^{\infty} V(\boldsymbol{b},w)dw} - 1\right] = \frac{ik}{m}\left[e^{i\chi(\boldsymbol{b})} - 1\right] \tag{13.47}$$

となる．ここで

$$\chi(\boldsymbol{b}) = -\frac{m}{k}\int_{-\infty}^{\infty} V(\boldsymbol{b},w)dw \tag{13.48}$$

と置いた．また $\Gamma(b)$ を

$$\Gamma(\boldsymbol{b}) \equiv 1 - e^{i\chi(\boldsymbol{b})} \tag{13.49}$$

と定義すると散乱振幅 $f(q)$ は

$$f(\boldsymbol{q}) = \frac{ik}{2\pi}\int d^2b\, e^{i\boldsymbol{q}\cdot\boldsymbol{b}}\,\Gamma(\boldsymbol{b}) \tag{13.50}$$

となっている．この $\Gamma(b)$ は profile function と呼ばれている．

13.4.1 Optical Theorem

散乱理論において Optical Theorem はかなり重要な役割を果たしている場合が多い．これはこの定理が散乱 S 行列の Unitarity と関係している事に依っている．ここでは Eikonal 近似によって求められた散乱振幅 $f(\boldsymbol{q})$ が Optical Theorem を満たしている事を証明しよう．散乱振幅 $f(\boldsymbol{q})$ は

$$f(\boldsymbol{q}) = \frac{ik}{2\pi}\int d^2b\, e^{i\boldsymbol{q}\cdot\boldsymbol{b}}(1-e^{i\chi(\boldsymbol{b})}) \tag{13.51}$$

であった．この場合，全断面積 σ_T は

$$\sigma_T = \int |f(\boldsymbol{q})|^2 d\Omega = \frac{1}{k^2}\int |f(\boldsymbol{q})|^2 d^2q \tag{13.52}$$

である．この上式に式 (13.51) の $f(\boldsymbol{q})$ を代入すると

$$\sigma_T = \frac{1}{k^2}\left(\frac{k}{2\pi}\right)^2 \int d^2q \int d^2b\, d^2b' e^{i\boldsymbol{q}\cdot(\boldsymbol{b}-\boldsymbol{b}')}(1-e^{i\chi(\boldsymbol{b})})(1-e^{-i\chi(\boldsymbol{b}')}) \tag{13.53}$$

となる．この式は $\boldsymbol{q}$ の積分を実行すると $[(2\pi)^2\delta(\boldsymbol{b}-\boldsymbol{b}')]$ が出てくるため，

$$\sigma_T = \int d^2b|(1-e^{i\chi(\boldsymbol{b})})|^2 = 2\int d^2b(1-\cos\chi(\boldsymbol{b})) \tag{13.54}$$

となっている．一方，$\mathrm{Im\,f}(0)$ は式 (13.51) から

$$\mathrm{Im} f(0) = \frac{k}{2\pi}\int d^2b\,(1-\cos\chi(\boldsymbol{b})) \tag{13.55}$$

となる．これより

$$\sigma_T = \frac{4\pi}{k}\,\mathrm{Im} f(0) \tag{13.56}$$

となる．これは Optical Theorem である．従って Eikonal 近似によって求められた散乱振幅 $f(q)$ は Optical Theorem を満たしている．恐らくこのため，Glauber 理論が予想以上にうまく実験を再現していると考えられるものである．

13.5　多重散乱理論

これまで扱ってきた散乱理論はポテンシャル散乱であり，これは１体問題の散乱理論である．実際には，例えば陽子が原子核と散乱する場合，これは多重散乱となっている．一般的に言って，多重散乱を理論的にきちんと扱う事は不可能である．しかしながら，多重散乱理論の記述に関しては Glauber 理論ではある程度の成功は収めているといえよう．それでここでは Glauber 理論について簡単に解説しよう．

13.5.1　高エネルギー陽子ー陽子散乱

まず高エネルギーにおける陽子ー陽子散乱の断面積を Eikonal 近似による散乱振幅 $f_{pp}(\boldsymbol{q})$ によって再現しよう．陽子ー陽子散乱の微分断面積は

$$\frac{d\sigma}{d\Omega} = |f_{pp}(\boldsymbol{q})|^2 \tag{13.57}$$

と書けるが，この時, 散乱振幅 $f_{pp}(\boldsymbol{q})$ は

$$f_{pp}(\boldsymbol{q}) = \frac{ik}{2\pi}\int d^2b\, e^{i\boldsymbol{q}\cdot\boldsymbol{b}}\,\Gamma_{pp}(\boldsymbol{b}) \tag{13.58}$$

となっている．ここで $\Gamma_{pp}(\boldsymbol{b})$ は

$$\Gamma_{pp}(\boldsymbol{b}) = 1 - e^{i\chi(\boldsymbol{b})} \tag{13.59}$$

である．高エネルギーにおける陽子ー陽子散乱の断面積の実験を再現するために

$$\Gamma_{pp}(\boldsymbol{b}) = C_0 e^{-\frac{1}{2}p_0^2\boldsymbol{b}^2} \tag{13.60}$$

と仮定する場合が良くある．$C_0,\ p_0$ は定数である．この場合, 散乱振幅は

$$f_{pp}(\boldsymbol{q}) = \frac{ik}{2p_0^2}C_0\, e^{-\frac{1}{2}\frac{\boldsymbol{q}^2}{p_0^2}} \equiv f_{pp}(0)\, e^{-\frac{1}{2}\frac{\boldsymbol{q}^2}{p_0^2}} \tag{13.61}$$

となっている．ここで $f_{pp}(0)$ は定数である．今の場合，Optical Theorem を満たすようにすると

$$f_{pp}(0) = \frac{(i+a_0)k\sigma_T}{4\pi} \tag{13.62}$$

と書く事が出来る．a_0 は実験値を再現するように決められるパラメータである．

13.5.2 高エネルギー陽子ー原子核散乱

多重散乱の最も単純な場合として高エネルギーの陽子ー原子核の弾性散乱の微分断面積を計算しよう．この場合，基礎になる散乱振幅は陽子ー陽子の散乱振幅 $f_{pp}(\boldsymbol{q})$ である．原子核は A 個の核子から成り立っていると仮定しよう．そしてその状態関数は最も単純化したものとして

$$\Psi_A(\boldsymbol{r}_1, \cdots, \boldsymbol{r}_A) = \phi_{n_1}(\boldsymbol{r}_1) \cdots \phi_{n_A}(\boldsymbol{r}_A) \tag{13.63}$$

としよう．これは反対称性も考慮していないので現実的なものではないが，まずは原子核反応論を優先して計算を進めて行こう．

13.5.3 Glauber 理論

問題は散乱における多体の効果をどのように計算できるかと言う事である．ここでは Glauber が提案した理論を紹介しよう．これは半世紀以上前の論文であるが，しかし前方散乱の実験を良く再現できる理論模型である．

高エネルギーの陽子ー原子核の弾性散乱において陽子ー原子核の散乱振幅 $f_A(\boldsymbol{q})$ は

$$f_A(\boldsymbol{q}) = \frac{ik}{2\pi} \int d^2b \, e^{i\boldsymbol{q}\cdot\boldsymbol{b}} \, \langle \Psi_A(\boldsymbol{r}_1, \cdots, \boldsymbol{r}_A) | 1 - e^{i\chi_A(\boldsymbol{b}, \boldsymbol{s}_1, \cdots, \boldsymbol{s}_A)} | \Psi_A(\boldsymbol{r}_1, \cdots, \boldsymbol{r}_A) \rangle \tag{13.64}$$

と書けると仮定している．ここで $\chi_A(\boldsymbol{b}, \boldsymbol{s}_1, \cdots, \boldsymbol{s}_A)$ は陽子と原子核の散乱における『位相』に対応するものである．この場合，s_i は横方向に対応する核子の座標を表している．すなわち $\boldsymbol{r}_i = (\boldsymbol{s}_1, z_i)$ である．

ここで多重散乱の効果を具体的に取り入れるため，前方散乱である事を考慮して次のような仮定をしよう．それはこの $\chi_A(\boldsymbol{b}, \boldsymbol{s}_1, \cdots, \boldsymbol{s}_A)$ が陽子ー核子散乱の和で書けるとするものである．すなわち

$$\chi_A(\boldsymbol{b}, \boldsymbol{s}_1, \cdots, \boldsymbol{s}_A) = \sum_{i=1}^{A} \chi_{pp}(\boldsymbol{b} - \boldsymbol{s}_i) \tag{13.65}$$

である．これは直感的に言えば，核子との散乱による位相のズレはそれぞれの核子との散乱によるものを足して行けば良いと言う仮定である．恐らく，前方散乱の場合，この仮定はそれ程，悪くはないものと考えられる．

13.5.4 陽子ー原子核の散乱断面積

これらの仮定の下で陽子ー原子核の散乱振幅 $f_A(\boldsymbol{q})$ を計算しよう．今の場合，散乱振幅 $f_A(\boldsymbol{q})$ は

$$f_A(\boldsymbol{q}) = \frac{ik}{2\pi}\int d^2b\, e^{i\boldsymbol{q}\cdot\boldsymbol{b}} \left(1 - \prod_{i=1}^{A}\left(1 - \int d^3r_i\, \rho_{n_i}(\boldsymbol{r}_i)\Gamma_{pp}(\boldsymbol{b}-\boldsymbol{s}_i)\right)\right) \qquad (13.66)$$

と書く事が出来る．ここで

$$\rho_{n_i}(\boldsymbol{r}_i) \equiv |\phi_{n_i}(\boldsymbol{r}_i)|^2 \qquad (13.67)$$

と定義されている．式 (13.66) を具体的に計算できる形にするため，さらに近似をして行こう．その近似とは $\rho_{n_i}(\boldsymbol{r}_i)$ が状態にはあまり依らないと言うものである．従って $\rho_{n_i}(\boldsymbol{r}_i)$ を原子核の密度関数 $\rho(\boldsymbol{r})$ で

$$\rho_{n_i}(\boldsymbol{r}) = \frac{1}{A}\rho(\boldsymbol{r}) \qquad (13.68)$$

と置き換える．但し，今の場合

$$\int d^3r\rho(\boldsymbol{r}) = A \qquad (13.69)$$

である．従って式 (13.66) は

$$f_A(\boldsymbol{q}) = \frac{ik}{2\pi}\int d^2b\, e^{i\boldsymbol{q}\cdot\boldsymbol{b}} \left(1 - \left(1 - \frac{1}{A}\int d^3r\, \rho(\boldsymbol{r})\Gamma_{pp}(\boldsymbol{b}-\boldsymbol{s})\right)^A\right) \qquad (13.70)$$

となる．ここで数学の恒等式

$$\left(1 - \frac{1}{A}\alpha\right)^A \simeq e^{-\alpha} \qquad (A \to \infty \text{ の時}) \qquad (13.71)$$

を利用しよう．この場合，式 (13.70) は

$$f_A(\boldsymbol{q}) = \frac{ik}{2\pi}\int d^2b\, e^{i\boldsymbol{q}\cdot\boldsymbol{b}} \left(1 - e^{-\int d^3r\, \rho(\boldsymbol{r})\Gamma_{pp}(\boldsymbol{b}-\boldsymbol{s})}\right) \qquad (13.72)$$

となる．実際の原子核の A は１０以上なので近似はかなり良いと言える．例として $A=20,\ \alpha=0.3$ として式 (13.71) を計算すると (左辺=0.739，右辺=0.741) となり，充分良い近似である事が分かる．

ここで $\Gamma_{pp}(\boldsymbol{b})$ を散乱振幅 $f_{pp}(\boldsymbol{q})$ で書いて見よう．これは Fourier 変換すると

$$\Gamma_{pp}(\boldsymbol{b}) = \frac{1}{2\pi ik}\int d^2q\, e^{-i\boldsymbol{q}\cdot\boldsymbol{b}}\, f_{pp}(\boldsymbol{q}) \tag{13.73}$$

と求まる．この式を使って式 (13.72) の右辺の積分を書き換えてみよう．この場合

$$\int d^3r\,\rho(\boldsymbol{r})\Gamma_{pp}(\boldsymbol{b}-\boldsymbol{s}) = \frac{1}{2\pi ik}\int d^2q\, d^3r\, e^{-i\boldsymbol{q}\cdot(\boldsymbol{b}-\boldsymbol{s})}\, f_{pp}(\boldsymbol{q})\,\rho(\boldsymbol{r}) \tag{13.74}$$

$$\simeq \frac{2\pi}{ik} f_{pp}(0)\int dz\,\rho(\boldsymbol{b},z) \tag{13.75}$$

となる．ここで前方散乱なので $\boldsymbol{q}=0$ の散乱振幅 $f_{pp}(0)$ が主として効いてくると仮定して， $f_{pp}(0)$ を積分から外すと言う近似を使っている．また $T(b)$ を

$$T(\boldsymbol{b}) = \int dz\,\rho(\boldsymbol{b},z) \tag{13.76}$$

として導入すると，陽子ー原子核散乱の散乱振幅は

$$f_A(\boldsymbol{q}) = \frac{ik}{2\pi}\int d^2b\, e^{i\boldsymbol{q}\cdot\boldsymbol{b}}\left(1-e^{-\frac{2\pi}{ik}f_{pp}(0)\,T(\boldsymbol{b})}\right) \tag{13.77}$$

となる．一方，散乱振幅 $f_{pp}(0)$ は

$$f_{pp}(0) = \frac{(i+a_0)k\sigma_{pp}^T}{4\pi} \tag{13.78}$$

と与えられているので，式 (13.77) は

$$f_A(\boldsymbol{q}) = \frac{ik}{2\pi}\int d^2b\, e^{i\boldsymbol{q}\cdot\boldsymbol{b}}\left(1-e^{-\frac{1}{2}\sigma_{pp}^T T(\boldsymbol{b})}\right) \tag{13.79}$$

と書けている．但しここでは a_0 項を省略している．従って陽子ー原子核弾性散乱の微分断面積は

$$\frac{d\sigma}{d\Omega} = |f_A(\boldsymbol{q})|^2 = \frac{k^2}{4\pi^2}\left|\int d^2b\, e^{i\boldsymbol{q}\cdot\boldsymbol{b}}\left(1-e^{-\frac{1}{2}\sigma_{pp}^T T(\boldsymbol{b})}\right)\right|^2 \tag{13.80}$$

となっている．

2.L

Nuclear Physics **A343** (1980) 493–510 © *North-Holland Publishing Co., Amsterdam*
Not to be reproduced by photoprint or microfilm without written permission from the publisher

MOMENTUM DISTRIBUTIONS AFTER FRAGMENTATION IN NUCLEUS-NUCLEUS COLLISIONS AT HIGH ENERGY†

T. FUJITA* and J. HÜFNER

Institut für Theoretische Physik der Universität Heidelberg
and
Max-Planck-Institut für Kernphysik, Heidelberg, Federal Republic of Germany

Received 13 December 1979

Abstract: We analyse the results of the experiment $^4He + target \rightarrow {}^3He + X$ at 1 GeV/nucl. We concentrate on the "spectator peak", where the velocity of the final fragment ^3He is equal to or larger than the projectile velocity. The shape and absolute value of the cross section can be understood quantitatively. Several effects contribute to the cross section in the transverse direction. But the ^3He fragments emitted at 0° reflect pure spectator physics: the momentum distribution of the observed ^3He is related in a simple way to the momentum distribution in ^4He. Using the experimental fragmentation cross section at 0° we deduce the shape of the momentum space wave function for the relative neutron-^3He motion inside ^4He.

1. The spectator peak

The work which we present here was started after we had seen the results of the fragmentation experiment

$$^4\mathrm{He} + \mathrm{target} \rightarrow {}^3\mathrm{He} + \mathrm{X}\,. \tag{1.1}$$

Anderson *et al.* [1]) have performed the experiment at the Bevalac at energies between 0.4 and 2.1 GeV/nucl. The momenta of the outgoing ^3He fragments are measured while everything else remains unobserved. The data exhibit a characteristic peak in the cross section at momenta where the velocities of the ^3He fragment and the ^4He projectile coincide. This peak will be called the "spectator peak" with the following idea in mind: this peak arises in the reaction (1.1) because the neutron is ripped off the projectile while the remaining ^3He fragment continues its motion essentially without being disturbed. To the degree to which this idea is correct, the momentum distribution of the ^3He in the spectator peak reflects the momentum distribution of the relative motion of the neutron–^3He inside the ^4He *before* the collision. Therefore an analysis of the spectator peak could be a way to measure intrinsic momenta, i.e. the nuclear wave function in momentum space (which is not the form factor!).

† Supported in part by a grant from the German Federal Ministry for Research and Technology (BMFT).

* Present address: Schweizer Institut für Nuklearforschung (SIN), CH-5234 Villingen, Switzerland.

Spectator peaks have already been observed in earlier experiments: Bizard *et al.* [2]) study the fragmentation reaction eq. (1.1) with protons as target. Greiner *et al.* [3]) map the shape of the peak for ^{12}C and ^{16}O projectiles. Compared to these experiments Anderson's measurement covers a considerably wider range of ^{3}He momenta. Some common basic features of the spectator peak appear in all experiments. These properties become particularly simple in the projectile rest system. Let us denote by $\boldsymbol{k} = (\boldsymbol{k}_\perp, k_\parallel)$ the momentum of the ^{3}He in this system ($k_\parallel$ being the component in beam direction and $\boldsymbol{k}_\perp$ the transverse components). Then the experimental fragmentation cross section for the reaction (1.1) shows the following features:

(a) In the neighborhood of the maximum the spectator peak is symmetric and can be parametrized by a Gaussian

$$E\frac{d\sigma}{d^3k} = \sigma_0\, e^{-k/k_0^2} \quad \text{for} \quad |\boldsymbol{k}| \leq 2k_0, \tag{1.2}$$

with $k_0 = 110$ MeV/c. For values $|\boldsymbol{k}| > 2k_0$ the shape becomes asymmetric, the cross section falls faster in longitudinal direction ($\boldsymbol{k}_\perp = 0$) than the transverse one ($k_\parallel = 0$), see fig. 1.

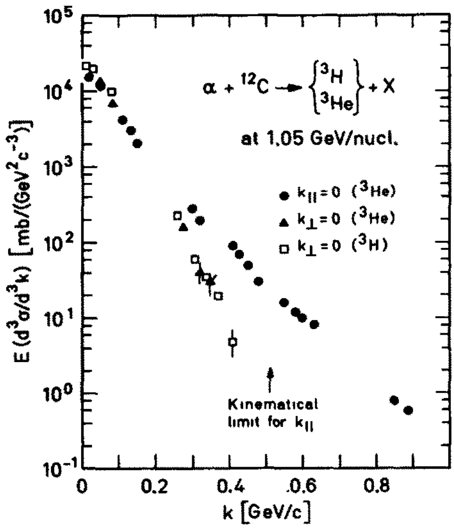

Fig. 1. The spectator peak for the fragmentation reaction $^4He + ^{12}C \rightarrow ^3He + X$. The experimental [1]) cross section $E\, d\sigma/d^3k$ with $\boldsymbol{k}$ as the ^3He momentum in the projectile rest frame is given for two cuts: Transverse to the beam direction (i.e. $k_\parallel = 0$) and in longitudinal direction ($k_\perp = 0$ and $k_\parallel > 0$). Note the symmetry for small k and the asymmetry for large k.

(b) The width k_0 does not depend on the target or on the energy, but is characteristic for the projectile. The integrated cross section in the peak is about 20 mb for hydrogen and 80 mb for Pb as targets and is independent of energy.

These properties seem to support the spectator idea: The magnitude and shape do not depend on the projectile energy as expected if the peak reflects intrinsic properties. The r.m.s. momentum $\langle \boldsymbol{p}^2\rangle^{1/2}$ for the n-^{3}He motion can be estimated from the r.m.s. charge radius $\langle \boldsymbol{r}^2\rangle_{ch}$ of ^{4}He to

$$\langle \boldsymbol{p}^2\rangle^{1/2} = \tfrac{9}{8}\langle \boldsymbol{r}^2\rangle_{ch}^{-1/2} = 135\ \mathrm{MeV}/c\,. \tag{1.3}$$

This value agrees well with the r.m.s. momentum width of the spectator peak

$$\langle \boldsymbol{k}^2\rangle^{1/2} = \sqrt{\tfrac{3}{2}}k_0 = 130\ \mathrm{MeV}/c\,. \tag{1.4}$$

A similar analysis has been performed for the spectator peak with ^{16}O projectiles [Abul-Magd *et al.*[4])]. But the peak also shows features which do not fit into the spectator picture: the asymmetry in longitudinal and transverse directions, for instance. Since ^{4}He has spin zero, the intrinsic momentum distribution is necessarily isotropic and the asymmetry must arise during the fragmentation process. The clue to understanding the asymmetry may be found in the analysis by Bizard *et al.* [2]): These authors observe that ^{3}He fragments at large transverse momenta have been scattered off the target. Therefore those ^{3}He fragments are "participants" rather than spectators. Obviously the physics of the spectator peak is not clear-cut and a careful analysis of the reaction mechanism seems to be called for. This analysis is the aim of this paper. We give a short summary of the results.

The cross section for the fragmentation is decomposed into three terms

$$E\frac{\mathrm{d}\sigma}{\mathrm{d}^3k} = E\left(\frac{\mathrm{d}\sigma}{\mathrm{d}^3k}\right)^{\mathrm{EF}} + E\left(\frac{\mathrm{d}\sigma}{\mathrm{d}^3k}\right)^{\mathrm{SP}} + E\left(\frac{\mathrm{d}\sigma}{\mathrm{d}^3k}\right)^{\mathrm{KO}}, \tag{1.5}$$

which correspond to "elastic fragmentation" (EF, the ^{4}He breaks up but the target remains in the ground state), to the "spectator" reaction (SP, a neutron of ^{4}He interacts inelastically with the target while the ^{3}He continues its path unaffected) and to the "knock-out" reaction (KO, the ^{3}He interacts inelastically with the target and receives momentum). The three processes are depicted in fig. 2. The spectator term always dominates the cross section under 0°, i.e. for $\boldsymbol{k}_\perp = 0$. In the transverse direction, the spectator cross section is most important at small momenta, but the knock-out cross section determines the behaviour for large $|\boldsymbol{k}_\perp|$ and is mainly responsible for the asymmetry.

To our knowledge there is only one paper which directly deals with reaction (1.1): Bizard *et al.*[5]) calculate the break-up for protons as the target (here only elastic fragmentation is possible) and put the emphasis on finite angles (large $k_\perp$). Several papers treat deuteron break-up: Fäldt *et al.* [6]), Bertocchi *et al.* [7]) and most recently Nissen-Meyer *et al.* [8]). These calculations are similar in spirit to ours, but mostly concentrate on finite transverse momenta. The careful analysis of the 0° cross section and its relation to the intrinsic wave function seem novel.

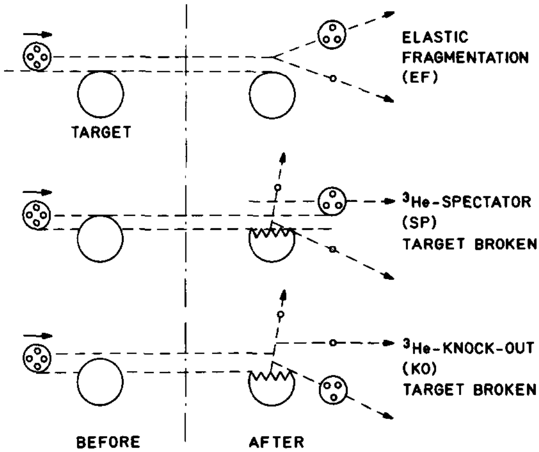

Fig. 2. Schematic drawing of the three processes which contribute to the fragmentation reaction in our analysis.

2. Analysing the fragmentation reaction within Glauber theory

We wish to understand the details of the fragmentation process before we calculate cross sections. Glauber's multiple scattering formalism [9]) provides an excellent guide. it is a non-perturbative theory, i.e. goes beyond the impulse approximation, yet it remains relatively simple: cross sections can be obtained in a closed form. However, energy conservation is violated and must be included in the theory before calculations are performed (sect. 3). In order to be specific we treat reaction (1.1) with ^{4}He as the projectile, but the results are easily generalized to other projectiles.

As explained in the introduction, the projectile rest frame seems to be the system in which the physics is most simple. Therefore we perform the calculation in this frame. Our notation is summarized in the following equation:

$$^4\text{He}\,\{|\Phi_0\rangle\} + \text{target}\,\{|-\boldsymbol{P}_0,\, T_0\rangle\}$$
$$\rightarrow {}^3\text{He}\,\{|\boldsymbol{k},\, h_0\rangle\} + \text{n}\{|\boldsymbol{k}_1\rangle\} + \text{target}'\ \{|-\boldsymbol{P}_0 - \boldsymbol{q},\, T\rangle\}\,. \tag{2.1}$$

In the projectile rest frame the ^{4}He has the intrinsic wave function $|\Phi_0\rangle$. The target (intrinsic wave function $|T_0\rangle$) arrives with momentum $-\boldsymbol{P}_0$. During the reaction the ^{4}He breaks up into a ^{3}He nucleus (momentum $\boldsymbol{k}$ and wave function $|h_0\rangle$) and a neutron with momentum $\boldsymbol{k}_1$. The target has received momentum transfer $-\boldsymbol{q}$ and is excited into the state $|T\rangle$. The wave function of relative motion between the ^{3}He and the neutron after break-up is denoted by $\chi_{\boldsymbol{p}}$, normalized as $\langle\chi_{\boldsymbol{p}}|\chi_{\boldsymbol{p}'}\rangle = \delta^{(3)}(\boldsymbol{p}-\boldsymbol{p}')$.

With this notation, the cross section for the fragmentation reaction eq. (2.1) is written in Glauber theory as

$$\frac{\mathrm{d}\sigma}{\mathrm{d}^3p\,\mathrm{d}^2q} = \left|\int \frac{\mathrm{d}^2b}{2\pi}\,\mathrm{e}^{-i\boldsymbol{q}\cdot\boldsymbol{b}}\langle\chi_{\boldsymbol{p}}h_0;T|1 - \prod_{\substack{i\in \mathrm{P}\\ j\in \mathrm{T}}}(1-\Gamma_{ij})|\Phi_0;\,T_0\rangle\right|^2, \tag{2.2}$$

where the Γ_{ij} are the profile functions for the collision between a nucleon i from the projectile and a nucleon j from the target. They are related to the nucleon-nucleon scattering amplitude by a Fourier transform,

$$f_{\mathrm{NN}}(\boldsymbol{q}) = \frac{i}{2\pi} \int \mathrm{d}^2 b \, \mathrm{e}^{-i\boldsymbol{q}\cdot\boldsymbol{b}} \, \Gamma(\boldsymbol{b}) \,. \tag{2.3}$$

In the fragmentation experiment, the ^{4}He breaks up; this fact is translated into the formalism by requiring the final n-^{3}He state to be orthogonal to the initial ground state of ^{4}He,

$$\langle \chi_p h_0 | \Phi_0 \rangle = 0 \,. \tag{2.4}$$

This relation has important consequences which will be discussed in detail later. In the experiment neither the final state of the target $|T\rangle$ nor the momentum transfer $\boldsymbol{q}$ are observed. Instead one measures the momentum $\boldsymbol{k}$ of the ^{3}He in the rest system of ^{4}He. From momentum conservation.

$$\boldsymbol{q} = \boldsymbol{k}_1 + \boldsymbol{k}, \qquad \boldsymbol{p} = \frac{3}{4}\boldsymbol{k}_1 - \frac{1}{4}\boldsymbol{k} \,. \tag{2.5}$$

The cross section eq. (2.2) has to be summed over all unobserved information before it can be compared to the experiment. The final formula is

$$\begin{aligned} \frac{\mathrm{d}\sigma}{\mathrm{d}^3 k} &= \int \mathrm{d}^2 q \int \mathrm{d}^3 p \, \delta^{(3)}(\tfrac{3}{4}\boldsymbol{q} - (\boldsymbol{k} + \boldsymbol{p})) \sum_T \frac{\mathrm{d}\sigma}{\mathrm{d}^3 p \, \mathrm{d}^2 q} \\ &= \int \mathrm{d}^2 q \sum_T \left| \int \frac{\mathrm{d}^2 b}{2\pi} \mathrm{e}^{-i\boldsymbol{q}\cdot\boldsymbol{b}} \langle \chi_{\frac{3}{4}\boldsymbol{q}-\boldsymbol{k}} h_0;\, T | \Pi (1 - \Gamma_{ij}) | \phi_0;\, T_0 \rangle \right|^2 . \end{aligned} \tag{2.6}$$

We proceed to evaluate eq. (2.6). Spin degrees of freedom and baryonic excitations (production of real and virtual Δ resonances) are neglected. Furthermore, we shall often use not properly antisymmetrized wave functions.

The profile functions $\Gamma_{ij}(\boldsymbol{x}_i^\perp - \boldsymbol{x}_j^\perp)$ depend on the transverse components of the nucleon coordinates. If $\boldsymbol{R}_\alpha$ and $\boldsymbol{R}_\mathrm{T}$ are the c.m. positions of the ^{4}He and the target, respectively, then

$$\boldsymbol{x}_i - \boldsymbol{x}_j = (\boldsymbol{x}_i - \boldsymbol{R}_\alpha) - (\boldsymbol{x}_j - \boldsymbol{R}_\mathrm{T}) + \boldsymbol{R}_\alpha - \boldsymbol{R}_\mathrm{T} \,. \tag{2.7}$$

The impact parameter $\boldsymbol{b}$ which appears in eqs. (2.2) and (2.6) is defined as $\boldsymbol{b} = \boldsymbol{R}_\alpha^\perp - \boldsymbol{R}_\mathrm{T}^\perp$. The intrinsic coordinates in the target are denoted by $\boldsymbol{s}_j = \boldsymbol{x}_j - \boldsymbol{R}_\mathrm{T}$ and Jacobi coordinates are chosen for the projectile,

$$\begin{aligned} \boldsymbol{x}_1 - \boldsymbol{R}_\alpha &= \tfrac{3}{4}\boldsymbol{\xi}_1 \,, & \boldsymbol{x}_3 - \boldsymbol{R}_\alpha &= \tfrac{1}{2}\boldsymbol{\xi}_3 - \tfrac{1}{3}\boldsymbol{\xi}_2 - \tfrac{1}{4}\boldsymbol{\xi}_1 \,, \\ \boldsymbol{x}_2 - \boldsymbol{R}_\alpha &= \tfrac{2}{3}\boldsymbol{\xi}_2 - \tfrac{1}{4}\boldsymbol{\xi}_1 \,, & \boldsymbol{x}_4 - \boldsymbol{R}_\alpha &= -\tfrac{1}{2}\boldsymbol{\xi}_3 - \tfrac{1}{3}\boldsymbol{\xi}_2 - \tfrac{1}{4}\boldsymbol{\xi}_4 \,. \end{aligned} \tag{2.8}$$

The ground-state wave function Φ_0 of ^{4}He is expanded in a complete set $\{h_\alpha\}$ of ^{3}He intrinsic states,

$$\Phi_0(\xi_1, \xi_2, \xi_3) = \sum_\alpha \varphi_\alpha(\xi_1) h_\alpha(\xi_2, \xi_3) , \tag{2.9}$$

where the spectroscopic amplitudes φ_α are not necessarily normalized to one. All excited states of ^{3}He are particle unstable, and since the ground state of ^{3}He is observed, we approximate

$$\Phi_0(\xi_1, \xi_2, \xi_3) \simeq \varphi_0(\xi_1) h_0(\xi_2, \xi_3) . \tag{2.10}$$

Then h_0 appears on both sides of the matrix element in eq. (2.6) and the following short notation can be introduced

$$\begin{aligned} S_3(b - \tfrac{1}{4}\xi_1; [s_j]) &= \langle h_0 | \prod_{j\in T} \prod_{i=2}^{4} (1 - \Gamma_{ij}) | h_0 \rangle , \\ S_1(b + \tfrac{3}{4}\xi_1; [s_j]) &= \prod_{j\in T} (1 - \Gamma_{ij}) , \end{aligned} \tag{2.11}$$

where the $[s_j]$ are the coordinates in the target nucleus. The S-matrix operators S_3 and S_1 describe ^{3}He-target and neutron-target collisions, respectively. We introduce the notation eq. (2.11) into eq. (2.6) and evaluate the sum over $|T\rangle$,

$$\begin{aligned} \frac{d\sigma}{d^3k} = \int d^2q \int \frac{d^2b\, d^2b'}{(2\pi)^2} e^{-iq(b-b')} 2 \int d^3\xi\, d^3\xi'\, \chi_p^*(\xi)\varphi_0(\xi)\chi_p(\xi')\varphi_0^*(\xi') \\ \times \langle T_0 | S_1^*(b' + \tfrac{3}{4}\xi'; [s_j]) S_1(b + \tfrac{3}{4}\xi; [s_j]) S_3^*(b' - \tfrac{1}{4}\xi'; [s_j]) S_3(b - \tfrac{1}{4}\xi; [s_j]) | T_0 \rangle . \end{aligned} \tag{2.12}$$

The scattering function $|\chi_p\rangle(P = \frac{3}{4}q - k)$ is orthogonal to φ_0 because of relation (2.4). The factor of 2 arises since each of the two neutrons can contribute. In the following, we have to approximate eq. (2.12). We want to do it such that unitarity is preserved since it is an important element of any scattering theory. We explain unitarity for our case. In Glauber theory $(1 - \Gamma(b))$ is the S-matrix for nucleon-nucleon scattering and must satisfy

$$|1 - \Gamma(b)|^2 = 1 . \tag{2.13}$$

This equation implies $S_1^* S_1 = 1$ provided the arguments of S_1^* and S_1 are the same. This holds under the following condition: If the wave functions χ_p are plane waves (violating $\langle \chi_p | \varphi_0 \rangle = 0$!), the integration over d^2q in eq. (2.12) can be performed

$$\int d^2q\, e^{-iq\cdot(b-b')} \chi_{3q/4-k}(\xi) \chi_{3q/4-k}(\xi') = e^{ik\cdot(\xi-\xi')} \delta^{(2)}_{(\frac{3}{4}\xi'_\perp + b' - \frac{3}{4}\xi_\perp - b)} \tag{2.14}$$

and unitarity $S_1 S_1^* = 1$ applies.

We propose the following approximation scheme to eq. (2.12). The matrix element in eq. (2.12) is decomposed into two terms,

$$\langle S_1 S_1^* S_3 S_3^* \rangle = \langle S_3 S_3^* \rangle + \langle S_3 S_3^* (S_1 S_1^* - 1) \rangle \tag{2.15}$$

which is still exact. The bracket denotes expectation values with respect to $|T_0\rangle$. The first term is kept unchanged but we approximate the second one,

$$\langle S_3 S_3^* (S_1 S_1^* - 1)\rangle \simeq \langle S_3\rangle\langle S_3^*\rangle\langle S_1 S_1^* - 1\rangle . \tag{2.16}$$

Note that unitarity is preserved. The approximation eq. (2.16) seems necessary in order to arrive at numerically tractable formulae. Processes are neglected where the ^{3}He excites the target *and* the neutron collides with the target. These processes seem less probable because of geometric reasons. The r.h.s. of eq. (2.16) has the form of a distorted-wave Born approximation: The product $S_1 S_1^*$ is proportional to the cross section for a neutron-target collision. During the collision the ^{3}He should not break up. This is ensured by the factor $\langle S_3\rangle$ which is the probability amplitude for the ^{3}He not breaking up in the field of the target.

Eq. (2.16) is the main approximation. Its accuracy has not been checked. With the help of eq. (2.16) the matrix element in eq. (2.12) is written as a sum of three terms which, as will be shown, correspond to elastic fragmentation, spectator and knock-out reactions, respectively:

$$\begin{aligned}\langle S_1^* S_1 S_3^* S_3\rangle &= \langle S_1^*\rangle\langle S_1\rangle\langle S_3^*\rangle\langle S_3\rangle \\ &\quad + \langle S_3\rangle\langle S_3^*\rangle(\langle S_1^* S_1\rangle - \langle S_1^*\rangle\langle S_1\rangle) + (\langle S_3^* S_3\rangle - \langle S_3^*\rangle\langle S_3\rangle) . \end{aligned}\tag{2.17}$$

The matrix elements $\langle S_i\rangle$ have the target ground state on both sides. They are the S-matrix elements for elastic scattering. The expressions in the round brackets,

$$\langle S_i^* S_i\rangle - \langle S_i^*\rangle\langle S_i\rangle = \sum_{\alpha\neq 0} \langle T_0|S_i^*|T_\alpha\rangle\langle T_\alpha|Si|T_0\rangle , \tag{2.18}$$

clearly correspond to inelastic ($\alpha \neq 0$!) collisions with the target. For hydrogen as target (and neglecting Δ-degrees of freedom) there are no excited states of the target and only the first term in eq. (2.17) survives.

The cross section which corresponds to the first term in eq. (2.17) is

$$\frac{d\sigma^{EF}}{d^3k} = 2\int d^2q \left| \int d^2b\, d^3\boldsymbol{\xi}\, e^{-i\boldsymbol{q}\cdot\boldsymbol{b}} \langle S_3(\boldsymbol{b} - \tfrac{1}{4}\boldsymbol{\xi})\rangle\langle S_1(\boldsymbol{b} + \tfrac{3}{4}\boldsymbol{\xi})\rangle \chi^*_{\frac{1}{4}\boldsymbol{q}-\boldsymbol{k}}(\boldsymbol{\xi})\varphi_0(\boldsymbol{\xi}) \right|^2 . \tag{2.19}$$

According to the numerical calculation the elastic fragmentation cross section is not too important. The reason can be understood from eq. (2.19). The S-matrices vary over a range of the size of the target. $\boldsymbol{\xi}$ has the order of magnitude of the projectile. One might be tempted to neglect the $\boldsymbol{\xi}$-dependence in the $\langle S_i\rangle$ altogether. Then because of the orthogonality, eq. (2.19) gives zero. To arrive at a non-vanishing term we expand in powers of $\boldsymbol{\xi}$,

$$\begin{aligned}&\frac{1}{i}\ln\langle S_3(\boldsymbol{b} - \tfrac{1}{4}\boldsymbol{\xi})\rangle\langle S_1(\boldsymbol{b} + \tfrac{3}{4}\boldsymbol{\xi})\rangle \\ &\quad \equiv \chi_3^{opt}(\boldsymbol{b} - \tfrac{1}{4}\boldsymbol{\xi}) + \chi_1^{opt}(\boldsymbol{b} + \tfrac{3}{4}\boldsymbol{\xi}) \\ &\quad = \chi_3^{opt}(\boldsymbol{b}) + \chi_1^{opt}(\boldsymbol{b}) + \boldsymbol{\xi}(\tfrac{3}{4}\boldsymbol{\nabla}\chi_1 - \tfrac{1}{4}\boldsymbol{\nabla}\chi_3) ,\end{aligned}\tag{2.20}$$

with the optical phase shift functions χ^{opt}. For instance χ_3^{opt} is proportional to the optical potential for ^{3}He-target scattering. Since the ^{3}He-target optical potential is about 3 times as large as the neutron-target one, the term proportional to $\boldsymbol{\xi}$ is also rather small. Or in basic physics: in order to break the ^{4}He in the mean field of the target, the force on the neutron must be different from the one on the ^{3}He.

The other two terms in eq. (2.17) lead to cross sections of the form

$$\frac{d\sigma^{\text{SP}}}{d^3k} = 2\int d^2q\, F_{\text{SP}}(\boldsymbol{k}, \boldsymbol{q})|\langle S_3(\boldsymbol{b}_{\max})\rangle|^2 \frac{d\sigma}{d^2q}(\text{n}+\text{T}_0 \to \text{n}+\text{X}(\neq \text{T}_0)),$$
$$\frac{d\sigma^{\text{KO}}}{d^3k} = 2\int d^2q\, F_{\text{KO}}(\boldsymbol{k}, \boldsymbol{q})\frac{d\sigma}{d^2q}(^3\text{He}+\text{T}_0 \to {}^3\text{He}+\text{X}(\neq \text{T}_0)). \tag{2.21}$$

Here the cross sections for *inelastic* neutron-target or ^{3}He-target collisions are defined as

$$\frac{d\sigma}{d^2q}(^3\text{He}+\text{T}_0 \to {}^3\text{He}+\text{X}(\neq \text{T}_0)) = \int \frac{d^2b\, d^2b'}{(2\pi)^2} e^{-i\boldsymbol{q}(\boldsymbol{b}-\boldsymbol{b}')} \times \sum_{\alpha \neq 0} \langle T_0|S_3^*(\boldsymbol{b}')|T_\alpha\rangle\langle T_\alpha|S_3(\boldsymbol{b})|T_0\rangle, \tag{2.22}$$

and for the neutron-target inelastic scattering one obtains it by replacing S_3 by S_1. The cross sections eq. (2.22) can be taken from experiment or calculated according to the paper by Glauber *et al.* [10]). The form factors F_{SP} and F_{KO} are defined as

$$F_{\text{SP}}(\boldsymbol{k}, \boldsymbol{q}) = \left|\int d^3\xi\, \chi^*_{\frac{1}{4}\boldsymbol{q}-\boldsymbol{k}}(\boldsymbol{\xi})\, e^{i\frac{1}{4}\boldsymbol{q}\cdot\boldsymbol{\xi}}\varphi_0(\boldsymbol{\xi})\right|^2 \to \frac{1}{(2\pi)^3}|\tilde{\varphi}_0(\boldsymbol{k})|^2, \tag{2.23a}$$

$$F_{\text{KO}}(\boldsymbol{k}, \boldsymbol{q}) = \left|\int d^3\xi\, \chi^*_{\frac{1}{4}\boldsymbol{q}-\boldsymbol{k}}(\boldsymbol{\xi})\, e^{-i\boldsymbol{q}\cdot\boldsymbol{\xi}/4}\right|^2 \to \frac{1}{(2\pi)^3}|\tilde{\varphi}_0(\boldsymbol{k}-\boldsymbol{q})|^2. \tag{2.23b}$$

The arrow indicates the limit where χ is approximated by a plane wave. Here $\tilde{\varphi}_0$ denotes the Fourier transform of φ_0. The spectator form factor F_{SP} only appeared after the following approximation

$$\left|\int d^3\xi\, \chi(\boldsymbol{\xi})\, e^{-i\frac{1}{4}\boldsymbol{q}\cdot\boldsymbol{\xi}}\langle S_3(\boldsymbol{b}-\boldsymbol{\xi})\rangle\varphi_0(\boldsymbol{\xi})\right|^2 \simeq |\langle S_3(\boldsymbol{b}_{\max})\rangle|^2 F_{\text{SP}}, \tag{2.24}$$

which is true as long as the ^{3}He-target elastic S-matrix varies slowly over the extension of the bound state wave function φ_0. The impact parameter $\boldsymbol{b}_{\max}$ is the position where most of the cross section arises. There is one case, particularly important for the ^{4}He fragmentation, where the approximation (2.24) is exact; if the scattering wave is a plane wave, φ_0 is a Gaussian and one looks at 0°, i.e. $\boldsymbol{k} = (0, 0, k_\parallel)$. Then the left-hand side of eq. (2.24) is proportional to $|\tilde{\varphi}_0(k_\parallel)|^2$.

We discuss the physics of eqs. (2.21): For the sake of clarity we take the limits indicated in eqs. (2.23) where $\chi_p \to \exp(-i\boldsymbol{p}\cdot\boldsymbol{\xi})/(2\pi)^{3/2}$. Then

$$\frac{d\sigma^{SP}}{d^3k} = 2\frac{\sigma_0}{(2\pi)^3}|\tilde{\varphi}_0(\boldsymbol{k})|^2$$
$$\frac{d\sigma^{KO}}{d^3k} = 2\int d^2q \frac{|\tilde{\varphi}_0(\boldsymbol{k}-\boldsymbol{q})|^2}{(2\pi)^3}\frac{d\sigma}{d^2q}(^3\mathrm{He}+\mathrm{T}_0 \to {}^3\mathrm{He}+\mathrm{X}(\neq \mathrm{T}_0)) \tag{2.25}$$

The shape of the spectator cross section *directly* reflects the single-particle momentum distribution. Since, as will be shown in the next section, the spectator cross section dominates for small $\boldsymbol{k}$, and the symmetry of the spectator peak in longitudinal and transverse direction reflects the isotropy of the intrinsic motion. The relation between the width of the peak and the r.m.s. momentum of the wave function, eqs. (1.3) and (1.4) follows immediately from eq. (2.25). The height of the spectator peak is determined by σ_0, the total inelastic neutron-target cross section. At high energies, this cross section is determined by geometry (size of the target) and depends weakly on the energy, as observed for the spectator peak. For large k, i.e. $k > 200$ MeV/c, the spectator cross section still dominates the longitudinal momentum distribution whereas the knock-out cross section $d\sigma^{KO}/d^2k$ determines the transverse direction. Since the knock-out cross section is a folding of the intrinsic momentum space distribution with the inelastic cross section, $d\sigma^{KO}/d^3k$ falls off slower. The dominance of the spectator cross section in parallel direction and the importance of the knock-out process in transverse direction is the reason for the observed asymmetry. These arguments reproduce qualitatively all features of the spectator peak. The numerical calculation reported upon in the next section proves also the quantitative agreement with experiment.

3. The numerical calculation

Energy conservation is neglected in the Glauber approximation to multiple scattering. In many practical cases, e.g. elastic scattering, this neglect has little consequence. Not so for the fragmentation reaction studied in this paper. Energy conservation cuts in severely. For instance it introduces a kinematical limit for the momentum distribution $d\sigma/d^3k$ in the spectator peak. We derive it for the longitudinal direction. Energy-momentum balance for reaction eq. (1.1) is written in the laboratory system of reference:

$$^4\mathrm{He}\,[\boldsymbol{P}_4, E_4] + \mathrm{T}_0[\boldsymbol{O}, M_{\mathrm{T}_0}] \to {}^3\mathrm{He}\,[\boldsymbol{P}_3, E_4 - M] +$$
$$+(\mathrm{T}+\mathrm{n})\left[\boldsymbol{P}_4 - \boldsymbol{P}_3,\ M_{\mathrm{T}_0} + M + \frac{(\boldsymbol{P}_4-\boldsymbol{P}_3)^2}{2(M_{\mathrm{T}_0}+M)}\right], \tag{3.1}$$

where energy and momentum of each partner is given in brackets. In the kinematical limit the ^{3}He carries away the maximal kinetic energy. The target plus neutron forming a bound $A+1$ system, absorb the momentum difference $\boldsymbol{P}_4-\boldsymbol{P}_3$ but do not carry significant kinetic energy because of the large mass. A Lorentz transformation into the rest system of the projectile leads to the following kinematical limit:

$$k_{\parallel}^{\max}=\frac{E_4}{M_4}\left(\sqrt{(E_4-M)^2+M_3^2}-\frac{P_4}{E_4}(E_4-M)\right)\to\frac{7}{8}M \quad \text{for } E_4\to\infty\,. \tag{3.2}$$

Even if the projectile energy E_4 goes to infinity, the parallel momentum $K_{\parallel}$ of ^{3}He in the projectile rest system cannot exceed 800 MeV/c! More generally: If the projectile has A_P nucleons, the kinematical limit for the fragment with (A_P-1) nucleons is

$$k_{\parallel}^{\max}=\left(1-\frac{1}{2A_P}\right)M \quad \text{for } E_A\to\infty. \tag{3.3}$$

In the actual experiment, where the kinetic energy of the incident ^{4}He is 1 GeV/nucl, the kinematical limit is at 500 MeV/c. Since experimental points go up to 400 MeV/c, energy conservation must be handled carefully. We modify the expressions for the cross sections derived in the previous sections in the following way. Eqs. (2.19) or (2.21) are in the form

$$\frac{d\sigma}{d^3k}=\int d^2q\,|T(\boldsymbol{k},\boldsymbol{q})|^2\,, \tag{3.4}$$

where the $\boldsymbol{q}$-integration is performed in the transverse direction. We replace $\boldsymbol{q}$ by the three-dimensional vector of momentum transfer and introduce a delta function for energy conservation in the projectile rest frame:

$$\frac{d\sigma}{d^3k}=\int d^3q\,\beta_0\delta(E_T^f-E_T^i+\sqrt{M_3^2+\boldsymbol{k}^2}+\sqrt{M^2+(\boldsymbol{k}-\boldsymbol{q})^2}-M_4)|T(\boldsymbol{k},\boldsymbol{q})|^2\,. \tag{3.5}$$

Here $\beta_0=P_4/E_4$ is the velocity of the beam and E_T^i and E_T^f are the energies of the target before and after the reaction, respectively,

$$E_T^i=\sqrt{M_T^2+\boldsymbol{P}_0^2}\,,$$
$$E_T^f=\begin{cases}\sqrt{M_T^2+(\boldsymbol{P}_0+\boldsymbol{q})^2}\,, & \text{(EF)}\\ (A-n)\sqrt{M^2+(\boldsymbol{P}_0/A_T)^2}+\sum_{i=1}^{n}\sqrt{M^2+(\boldsymbol{P}/A_T+\boldsymbol{q}_i)^2} & \text{(KO or SP)}\,.\end{cases} \tag{3.6}$$

The final energy of the target depends on the particular process: For elastic fragmentation (EF) the target absorbes the momentum transfer $\boldsymbol{q}$ as a whole. For an inelastic case, n nucleons are knocked out of the target and share the momentum transfer $\boldsymbol{q}=\sum_i \boldsymbol{q}_i$. Eq. (3.6) gives the final energies of the target for the two cases. We neglect binding effects. It seems necessary to know the details of the final target state in order to treat energy conservation properly. This is not so, at least not at high energy where the difference

$$E_T^f - E_T^i = \beta_0 q_\parallel + O(\langle \boldsymbol{q}^2 \rangle / (P_0/A_T)^2) \tag{3.7}$$

is independent of the two forms of eq. (3.6) for E_T^f at least to leading order. Since $\langle \boldsymbol{q}^2 \rangle$ remains constant with increasing energy the correction decreases. In the present experiment we estimate the error to be few percent. We show the importance of energy conservation for the fragmentation reaction. We assume the matrix element $|T(\boldsymbol{k}, \boldsymbol{q})| = \text{const}$ and perform the q-integration in eq. (3.5) assuming $\boldsymbol{k}_\perp = 0$. The result called "phase space" is plotted in fig. 3 as a function of $k_\parallel$.

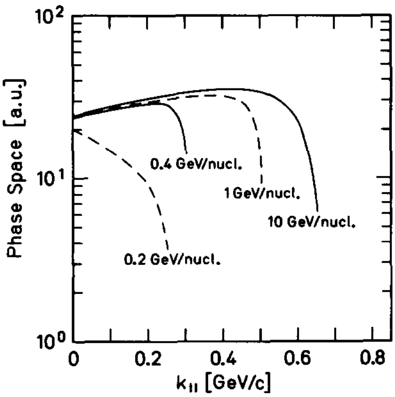

Fig. 3. The importance of energy conservation for the fragmentation reaction. The cross section is calculated by assuming the dynamical matrix element to be constant but taking energy conservation into account properly. This result is called phase space. It is plotted for different incident energies as a function of $k_\parallel$ for $k_\perp = 0$. Observe how abruptly the phase space drops.

The fragmentation reaction which we discuss is performed at high energy. It seems reasonable to neglect Coulomb effects. Furthermore one is tempted to assume all scattering wave functions to be plane waves. This is certainly correct for the incident wave (the ^{4}He-target relative motion), but dangerous for the relative motion between the ^{3}He and the neutron after break-up, since they move rather slowly relative to each other. For a typical momentum transfer $\langle \boldsymbol{q}^2 \rangle^{1/2} \simeq 400$ MeV/c to the neutron in the ^{3}He spectator process, the neutron energy is $\langle q^2 \rangle / 2M = 80$ MeV. A careful consideration of the ^{3}He final state interaction is also imposed by the orthogonality requirement eq. (2.4), which now reads

$$\langle \chi_p | \varphi_0 \rangle = 0\,. \tag{3.8}$$

We shall assume that the neutron after the break-up moves in the same potential V as the one that binds the neutron to the ^{3}He. Then the solutions of the Schrödinger equation for the bound state φ_0 and the scattering wave χ_p are automatically orthogonal. In order to avoid excessive numerical integrations, we assume the potential to be of separable form

$$\langle \boldsymbol{r}'|V|\boldsymbol{r}\rangle = \langle \boldsymbol{r}'|u\rangle\lambda\langle u|\boldsymbol{r}\rangle\,. \tag{3.9}$$

The strength λ is determined such that a bound state exists at the experimental value of the separation energy of ^{4}He ($E_B = -20$ MeV). The shape of $\langle \boldsymbol{T}|u\rangle$ is related to the bound state wave function φ_0 by

$$\tilde{u}(\boldsymbol{k}) \propto \left(E_B - \frac{k^2}{2M}\right)\tilde{\varphi}_0(k)\,. \tag{3.10}$$

Then the Lippmann-Schwinger equation for the scattering function in the potential eq. (3.9) can be solved analytically and is given by $k_B^2 = -2ME_B$,

$$(2\pi)^{-3/2}\langle \boldsymbol{k}|\chi_{\boldsymbol{p}}\rangle = \delta^{(3)}(\boldsymbol{k}-\boldsymbol{p}) - \frac{k^2+k_B^2}{k^2-p^2-i\varepsilon}\,\frac{\tilde{\varphi}_0(\boldsymbol{k})\tilde{\varphi}_0^*(\boldsymbol{p})}{\int d^3q|\tilde{\varphi}_0(\boldsymbol{q})|^2\dfrac{q^2+k_B^2}{q^2-p^2-i\varepsilon}}\,. \tag{3.11}$$

For the numerical calculations we have defined an "orthogonality defect" $C(\boldsymbol{p}, \boldsymbol{q})$ by

$$\tilde{\varphi}_0(\boldsymbol{p})C(\boldsymbol{p},\boldsymbol{q}) = \int d^3k\,\tilde{\varphi}_0(\boldsymbol{q}-\boldsymbol{k})[(2\pi)^{3/2}\langle \boldsymbol{k}|\chi_{\boldsymbol{p}}\rangle - \delta^{(3)}(\boldsymbol{p}-\boldsymbol{k})]\,. \tag{3.12}$$

For a Gaussian wave function $\tilde{\varphi}_0(\boldsymbol{p}) \propto \exp(-p^2/2p_0^2)$, a simple parametrization (which is better than 10%) has been found

$$C(\boldsymbol{p},\boldsymbol{q}) \simeq \exp\{-0.28(q/p_0)^2\exp(-0.27\,p/p_0)\}\,, \tag{3.13}$$

where we ignored the imaginary part of C eq. (3.12), which is found to be negligible.

The importance of the orthogonality corrections is shown in fig. 4. The cross sections for the fragmentation of ^{4}He are drawn for the elastic fragmentation part eq. (2.19) and for the spectator and knock-out process eq. (2.21). The comparison shows results with a proper neutron wave χ_p "orthogonalized wave" and with a plane wave. The size of the effect depends on the particular process: proper final-state interaction reduces the elastic fragmentation (EF) cross section by about a factor of 10. In this way the EF cross section is reduced from dominance to minor importance. The spectator cross section (SP) remains practically unaffected by the final-state interaction.

The potential V eq. (3.9) which we use to calculate the distortion has deficiencies: by construction it acts only in relative s-waves. Furthermore, it is a hermitian potential, while for positive energy of the outgoing neutron an absorptive part should be added. The absorptive part is responsible for a reduction of flux: The knocked-on neutron moves partly through the ^{3}He and may excite it on the way. In those cases there is no ^{3}He observed. From geometrical arguments we estimate the probability to be $\frac{1}{2}$ that the ^{3}He is destroyed by final-state interaction. Therefore we reduce all calculated cross sections by this factor $\frac{1}{2}$.

We close this section by giving the expressions for the various amplitudes and elementary cross sections which enter the final expressions for the fragmentation

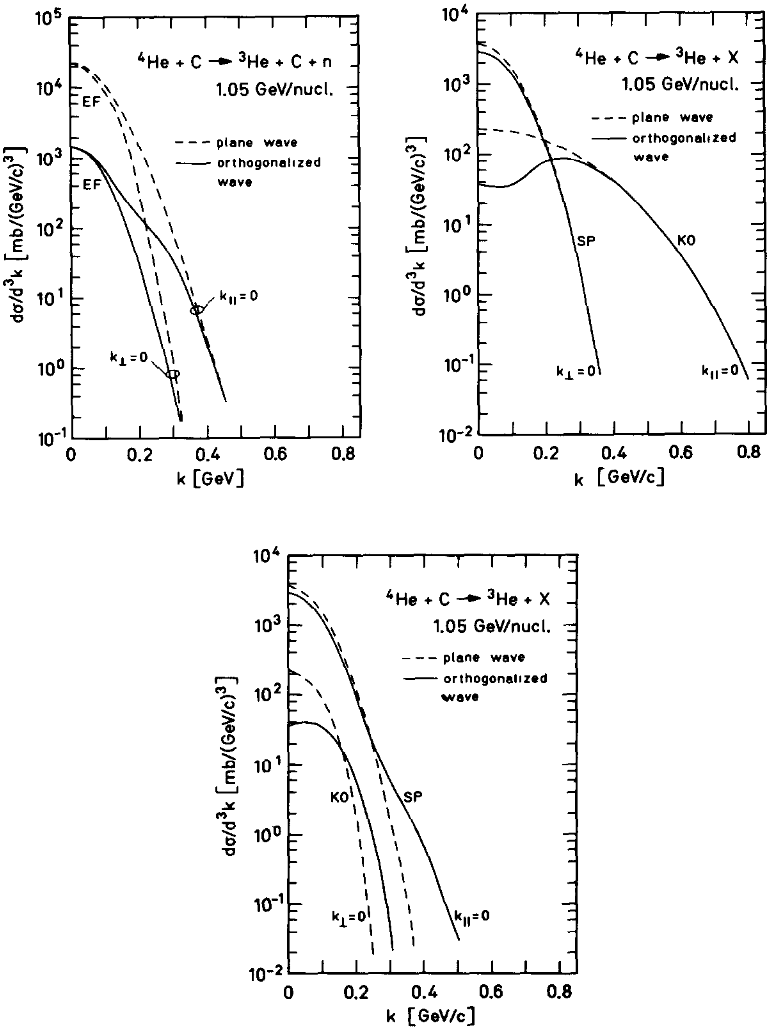

Fig. 4. The importance of the proper final-state interaction for the relative motion between neutron and ^{3}He after break-up. We show cross sections for selected processes (elastic fragmentation, "EF", etc.) calculated without and with the final-state interaction for the neutron-^{3}He relative motion ("plane wave" and "orthogonalized wave", respectively).

cross sections. Wherever possible, we employ Gaussians to simplify the numerical calculations. The bound state function for the relative n-^{3}He motion is a Gaussian with a Fourier transform

$$\tilde{\varphi}_0(\boldsymbol{k}) = \left(\frac{4\pi}{p_0^2}\right)^{3/4} e^{-k^2/2p_0^2}, \qquad (3.14)$$

whose width p_0 is obtained from the experimental charge radius of ^{4}He via eq. (1.3).

The elastic fragmentation cross section contains the S-matrices for elastic ^{3}He-target and for elastic n-target collisions. We choose $\langle S_i \rangle - 1$ to be Gaussians,

$$1-\langle S_i(b)\rangle = e^{-\frac{3}{2}b^2/R_i^2} . \qquad (3.15)$$

The radius constants R_i for ^{12}C as target are

$$\begin{aligned} R_1 &= 2.3 \text{ fm} \qquad (\text{n}-{}^{12}\text{C scattering}) \\ R_3 &= 3.1 \text{ fm} \qquad ({}^3\text{He}-{}^{12}\text{C scattering}) . \end{aligned} \qquad (3.16)$$

The radius R_1 is chosen to fit elastic $p-{}^{12}$C scattering at 1 GeV for not too large momentum transfer. The value of R_3 is deduced from the ^{4}He-^{12}C elastic cross section. The incoherent inelastic n-target and ^{3}He-target cross sections are parametrized in the form derived by Fujita *et al.* [11]), and they have been tested for the reaction ^{4}He + target → ^{4}He + X,

$$\frac{d\sigma}{d^2q}(\text{h} + {}^{12}\text{C} \to \text{h} + \text{X}(\text{not}\,{}^{12}\text{C}_{\text{y.s.}})) = \frac{L^2}{q_0^2} \sum_{n=1}^{A} \frac{1}{\varepsilon_i^n} \frac{1}{n^2} e^{-q^2/nq_i^2} , \qquad (3.17)$$

where $L^2 = 65$ mb and

$$\begin{aligned} \varepsilon_3 &= 3, \qquad q_3 = 200 \text{ MeV}/c \qquad ({}^3\text{He as projectile}) , \\ \varepsilon_1 &= 8, \qquad q_1 = 390 \text{ MeV}/c \qquad (\text{n as projectile}) . \end{aligned} \qquad (3.18)$$

The shadowing factor $|\langle S(b_{\max})\rangle|^2$ defined in eq. (2.24) for the spectator contribution has been included in eq. (3.17) by replacing $\varepsilon_1 = 2$ (which would be appropriate for $n-{}^{12}$C collision) by $\varepsilon_1 = 8$. The results of our calculation are compared with experiment in the next section.

4. The results and their discussion

The fragmentation cross section for the reaction ^{4}He + target → ^{3}He + X is decomposed into three terms

$$\frac{d\sigma}{d^3k} = \left(\frac{d\sigma}{d^3k}\right)^{\text{EF}} + \left(\frac{d\sigma}{d^3k}\right)^{\text{SP}} + \left(\frac{d\sigma}{d^3k}\right)^{\text{KO}} . \qquad (4.1)$$

They correspond to elastic fragmentation (EF, the target remains in the ground state) to the spectator part (SP, where the neutron is knocked out of ^{4}He and the ^{3}He continues unaffectedly) and to the knock-out process (KO, where the ^{3}He receives momentum during the collision). For a schematic representation see fig. 2. There are no free parameters in the theory. We compare the expressions with experiment. We start by elastic fragmentation. Its calculation is rather delicate, since amplitudes of opposite signs are added. Fortunately there is a case in which elastic fragmentation is the only contribution and can therefore be tested:

$$^4\text{He} + \text{p} \to {}^3\text{H} + \text{n} + \text{p} . \qquad (4.2)$$

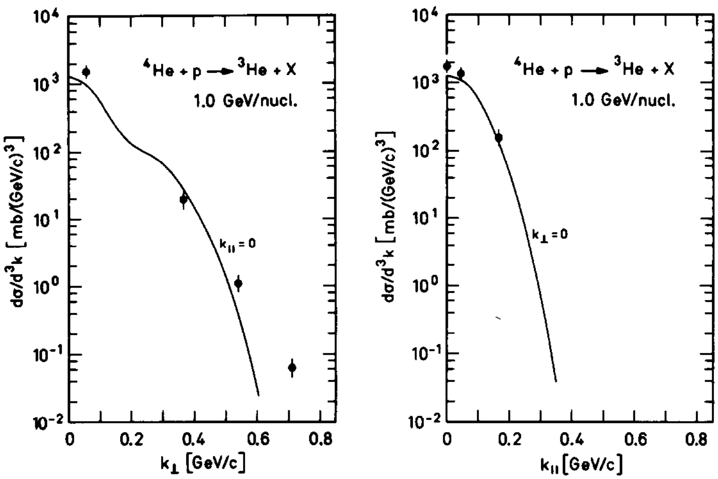

Fig. 5. The fragmentation reaction with proton as target. Here only elastic fragmentation contributes. Our calculation is compared with experimental results by Bizard *et al.* [2]).

Fig. 5 shows a comparison between our calculation and the experiment by Bizard *et al.* [2]). The basic features are understood: The absolute magnitude is reproduced within 50%. The narrow width in the longitudinal direction ($k_{\perp} = 0$) and the rather broad structure in the transverse direction ($k_{\parallel} = 0$) agree fairly well. Only for large $k_{\perp}$ a discrepancy develops. It is partly due to the Gaussian approximation for the elastic S-matrix like in eq. (3.15).

After being sure that elastic fragmentation is handled correctly, we can proceed to more complicated targets. Fig. 6 shows the experimental points for ^{12}C together with

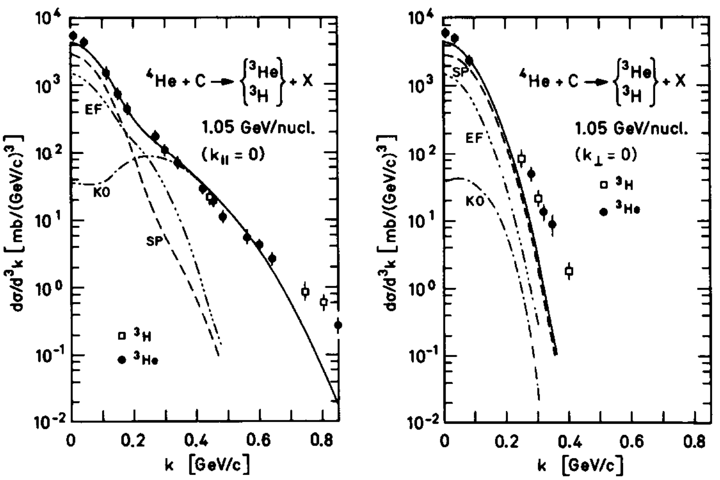

Fig. 6. The fragmentation reaction on ^{12}C as target. The experimental cross sections from Anderson *et al.* [1]) are compared with the calculation (solid curve). The broken lines show the various contributions (elastic fragmentation, EF, spectator process, SP, and knock-out reaction KO).

the calculation. The spectator term dominates in the longitudinal direction. The elastic fragmentation is smaller by at least a factor two and the knock-out process is completely unimportant. In transverse direction the situation is more complicated. Although the spectator term dominates at small momenta, the elastic fragmentation takes over in the intermediate regime and for large transverse momenta the knock-out process determines the cross section. The dominance of the spectator part at low momenta explains the symmetry of the fragmentation cross section in $k_\parallel$ and $k_\perp$. The increasing importance of the knock-out process is responsible for the asymmetry at large values of k. The overall agreement between experiment and calculation is good, but the comparison clearly reveals discrepancies, in particular for high momenta. We suspect the approximation eq. (2.16) to be partly responsible for the discrepancy in transverse direction since processes are neglected in which both neutron and ^{3}He interact inelastically. This may lead to high transverse momenta. Furthermore the shape in this domain depends critically on how well (experimentally) the condition $k_\parallel = 0$ is realized.

To our opinion, the discrepancy in the longitudinal direction is connected with the Gaussian approximation for the momentum distribution inside ^{4}He. We just do not see any other reason since all dynamical processes affect the transverse distribution. Therefore we turn the argument around: We look for a distribution $|\tilde{\varphi}_0(\boldsymbol{k})|^2$ whose corresponding cross section agrees with experiment in the longitudinal direction. Fortunately the relation between $|\tilde{\varphi}_0|^2$ and the cross section is simple for the spectator contribution which dominates for $k_\perp = 0$: The cross section is directly proportional to $|\tilde{\varphi}_0(\boldsymbol{k})|^2$, cf. eq. (2.25). This result is not changed by the final-state interaction, since distortion influences the spectator cross section $\mathrm{d}\sigma^{\mathrm{SP}}/\mathrm{d}^3k$ only in a minor way (fig. 4). Energy conservation, however, has to be handled carefully. The relation between calculated cross section and the momentum distribution is contained in the function

$$Z(k_\parallel) = \left(\frac{\mathrm{d}\sigma}{\mathrm{d}^3k}\right)_{\mathrm{calc}} \Big/ |\tilde{\varphi}(k_\parallel)|^2 , \tag{4.3}$$

where the calculated cross section contains all contributions including final state interaction. Fig. 7 shows the function Z. The correcting function Z is calculated for a Gaussian distribution $|\tilde{\varphi}_0|^2$. As suggested by relation eq. (2.25) for the spectator cross section, the function Z should be independent of $|\varphi_0|^2$. We assume this independence. Then an experimental momentum distribution can be extracted from the fragmentation cross section in longitudinal direction by

$$|\tilde{\varphi}_0(k_\parallel)|^2_{\mathrm{exp}} = \frac{\mathrm{d}\sigma}{\mathrm{d}^3k}(k_\perp = 0)|_{\mathrm{exp}}\, Z^{-1}(k_\parallel) . \tag{4.4}$$

The result is shown in fig. 8. As expected, the distribution follows the Gaussian for low momenta. Then it deviates and falls less rapidly. The reason is not clear to us: It may

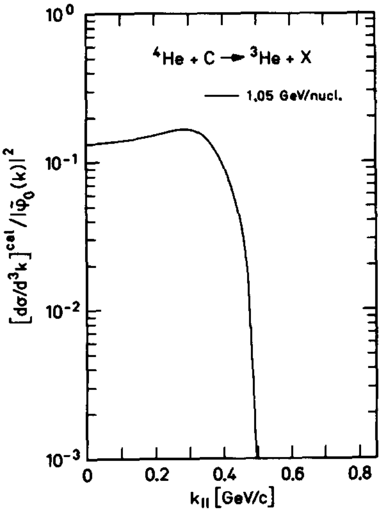

Fig. 7. The correcting function Z defined in eq. (4.3) as a function of the longitudinal momentum. Although the calculated cross section and the momentum distribution decay rapidly with increasing $k_\parallel$, the ratio is practically constant up to the kinematical limit.

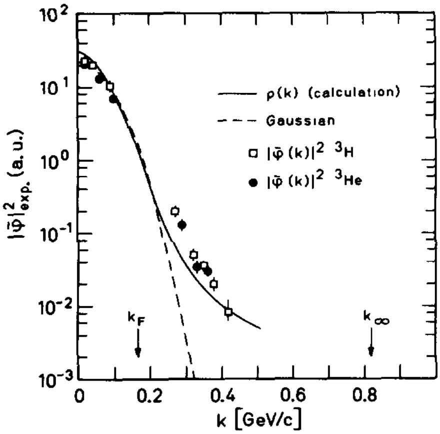

Fig. 8. The experimental momentum distribution of the neutron (proton) bound state wave function in ^{4}He. The points are computed from the experimental fragmentation cross section using the relation (4.4). The calculated momentum distribution is due to Zabolitzky *et al.* [12]). For orientation we indicate the Fermi momentum k_F for n-^{3}He relative motion and the kinematical limit k_∞ for infinite incident energy.

be due to nucleon-nucleon correlations. We do not know of any detailed experimental mapping of $|\varphi_0(k)|^2$ for ^{4}He. We are only aware of the calculation by Zabolitzky *et al.* [12]). These authors give $\rho(\boldsymbol{k})$, the probability to find a nucleon with momentum $\boldsymbol{k}$ inside ^{4}He. This quantity is different from $|\varphi_0(\boldsymbol{k})|^2$ which is the probability to find momentum $\boldsymbol{k}$ under the condition that ^{3}He remains in the ground state. More quantitatively, if the intrinsic wave function Φ of ^{4}He is expanded

$$\Phi(\xi_1, \xi_2, \xi_3) = \sum_{n=0}^{\infty} \varphi_n(\boldsymbol{\xi}_1) h_n(\boldsymbol{\xi}_2, \boldsymbol{\xi}_3) , \tag{4.5}$$

where the h_n are normalized to 1, then

$$\rho(\boldsymbol{k}) = \sum_{n=0}^{\infty} |\tilde{\varphi}_n(\boldsymbol{k})|^2 \geqq |\tilde{\varphi}_0(\boldsymbol{k})|^2 . \tag{4.6}$$

Although $\rho(\boldsymbol{k})$ and $|\tilde{\varphi}_0(\boldsymbol{k})|^2_{\text{exp}}$ need not be equal, the calculated momentum distribution agrees fairly well with $|\tilde{\varphi}_0|^2_{\text{exp}}$. In particular, the deviation from the Gaussian is reproduced. We do not know how significant the remaining discrepancies are.

We summarize: The fragmentation reaction ^{4}He + target → ^{3}He + X can be quantitatively understood in the spectator peak. The cross section at 0° is particularly interesting. it reflects in a simple way the momentum distribution inside the projectile nucleus. We think that a study of the spectator peak is a good way to measure intrinsic momenta. We close by warning: The fragmentation cross section for ^{4}He + target → p + X at 0° cannot easily be related to the momentum distribution inside the projectile. Final-state interactions influence magnitude and shape of the spectator peak considerably [13]).

We enjoyed many discussions with the colleagues and friends of the institute. We are especially grateful to J. Knoll whose advice and constructive criticism greatly improved the work. We thank S. Nagamiya and I. Sick for long discussions. Mrs. Einecke typed the manuscript and Mrs. Seitz drew the figures.

References

1) L. M. Anderson, Ph.D. thesis Sept. 1977, Report LBL 6769
2) G. Bizard, C. Le Brun, J. Berger, J. Duflo, L. Goldzahl, F. Plonin, J. Oostens, M. v. d. Bossche, L. Vu Hai, F. L. Fabbri, P. Picozza and L. Satta, Nucl. Phys. **A285** (1977) 461
3) D. E. Greiner, P. J. Lindstrom, H. H. Heckman, B. Cork and F. S. Beiser, Phys. Rev. Lett. **35** (1975) 152
4) A. Abul-Magd and J. Hüfner, Z. Phys. **A227** (1976) 379
5) G. Bizard and A. Tekou, Nuovo Cim., to be published
6) G. Fäldt and H. Pilkuhn, Ann. of Phys. **58** (1970) 454
7) L. Bertocchi and A. Tekou, Nuovo Cim. **21A** (1974) 223;
L. Bertocchi and D. Treleani, Nuovo Cim. **36A** (1976) 1
8) S. A. Nissen-Meyer, Nucl. Phys. **A306** (1978) 499;
J. H. Kühn and S. A. Nissen-Meyer, Nucl. Phys. **A312** (1978) 409
9) R. J. Glauber, Lectures in theoretical physics, Boulder, Colorado, 1958, ed. W. E. Brittin and L. G. Dunham, vol. I (Interscience, N.Y., 1959) p. 315
10) R. J. Glauber and G. Matthiae, Nucl. Phys. **B21** (1970) 135
11) T. Fujita and J. Hüfner, Phys. Lett. **87B** (1979) 327
12) J. Zabolitzky and W. Ey, Phys. Lett. **76B** (1978) 527
13) T. Fujita and J. Hüfner, Nucl. Phys. **A314** (1979) 317